Wireless Personal Communications **3:** 257–271, 1996.

A Coverage Prediction Technique for Indoor Wireless Millimeter Waves System

PAUL MARINIER, GILLES Y. DELISLE and LARBI TALBI
INRS-Télécommunications (Université du Québec), 16 place du commerce, Verdun, Qué., Canada H3E 1H6
(Tel.: 514 7658202; Fax: 514 7618501; E-mail: delisle@inrs-telecom.uquebec.ca)

Abstract. In view of the fact that future indoor wireless LAN's are likely to operate in the mm-wave region (20-60 GHz) due to spectrum availability and wider bandwidth requirements, site-specific coverage and channel dispersion prediction need to be made in order to allow maximum capacity in particular situations. This paper introduces a prediction technique which takes into account multiple reflections and diffraction phenomena in an user-specified environment. An efficient 3D ray tracing method is proven to accurately compute all significant paths between transmitter and receiver. Comparisons between predicted and measured results for both wideband and narrowband situations are presented and results show that this technique can be easily applicable in real system engineering.

Key words: Prediction techniques, millimeter waves, ray tracing, diffraction, experimental results.

1. Introduction

Because of its availability, the mm-wave region (20-60 GHz) is now allocated for the development of wireless indoor LAN's. The high data rates needed for simultaneous data, voice and image transmission make difficult, if not impossible, the implementation of these services in a system operating in the UHF band. Furthermore, the high spatial attenuation experienced by millimeter waves is suitable for a cellular-type architecture.

A significant amount of work has already been done to characterize the indoor radio channel in the UHF frequency band, under statistical or deterministic aspects [1–12]. The development of powerful computers during the last decade has allowed the use of high-frequency techniques (or ray techniques) to attempt a prediction of the channel parameters based on the structure and the electromagnetical properties of the propagation environment [3–12]. Various approaches address the problem of computing the most significant rays in a specified environment. For the majority of these useful studies, computation time still appears to be an important limiting factor to an efficient implementation of the models, forcing the elaboration of a faster scheme for ray tracing. Besides this, an acceptable agreement between prediction and measurements is seldom reached and this may be attributed in a great part to the lack of accurate information on the electrical properties of materials.

Characterization of the channel in the millimeter waves band has already begun with measurements as well as statistical and deterministic modeling [13–16]. The distinct behavior of millimeter waves from UHF waves imposes the use of different approaches for the prediction. It is generally recognized that transmission of energy through walls made up of materials like concrete or steel is significantly lower than in the UHF case. Whenever a building is partitioned with such walls, this reduces the size of the computation environment of interest from a complete floor (for UHF waves) to typically a few rooms. In that case, this may yield a significant role to diffraction phenomena when there is no direct path between the two terminals (a non-LOS situation). A prediction model proposed in [15] is already available and

it provides good results when the environment considered is a single simple-shaped room. However, this model cannot take into account the diffraction phenomena, which may become important in more complex geometries.

The study presented here allows to take care for multiple reflections and diffractions effects in an user-specified propagation environment. It is based on geometrical optics (GO) and uniform theory of diffraction (UTD). An original ray tracing algorithm has been elaborated to compute all significant paths between transmitter and receiver. The model can predict the channel impulse response for any positions of the antennas in the environment, and also the received power for each point of the environment (coverage map) for a given transmitter position. Comparisons with measured data show acceptable agreement between predicted and experimental results, considering the lack of information about material properties at the frequencies of interest.

2. Channel Characterization

2.1. Interaction Mechanisms

The interaction mechanisms of radiowaves with scatterers are usually classified as reflection, transmission and diffraction. In the case of millimeter waves (37.2 GHz) propagating in an indoor environment, measurements have shown [13] that transmission losses through concrete walls are generally in excess of 30 dB, while it is only a few dB in the UHF band. This model assumes that transmission through walls can be neglected and therefore does not apply to all kinds of environments. Some care must be taken to make sure that this assumption is reasonably satisfied. Reflection phenomena onto plane walls, floor and ceiling are obviously the most important and they are accounted for in this prediction technique. It is expected that the diffraction by vertical edges may yield weak albeit significant contributions, especially near shadow boundaries. Its relative importance is raised by the fact that no energy can propagate through the walls blocking the direct path between the source and the observation point. For this reason, diffraction by vertical edges has also be accounted for in the model.

2.2. Ray Techniques

The reflection and diffraction mechanisms can be conveniently described by the use of ray techniques, which consists in geometrical optics (GO) and uniform theory of diffraction (UTD). For the reflection case, the finite conductivity of walls can be taken into account by the use of the well-known Fresnel dyadic coefficient [17]:

$$R_{\perp} = \frac{\sin\psi - \sqrt{\hat{\epsilon}_r - \cos^2\psi}}{\sin\psi + \sqrt{\hat{\epsilon}_r - \cos^2\psi}} \tag{1}$$

$$R_{||} = \frac{\hat{\epsilon}_r \sin\psi - \sqrt{\hat{\epsilon}_r - \cos^2\psi}}{\hat{\epsilon}_r \sin\psi + \sqrt{\hat{\epsilon}_r - \cos^2\psi}} \tag{2}$$

$$\hat{\epsilon}_r = \epsilon_r - j\sigma/\omega\epsilon_0 \tag{3}$$

where $R_{\perp}$ and $R_{||}$ refer respectively to perpendicular and parallel polarizations, ψ is the angle between the incident ray and the surface, ϵ_r and σ are respectively the relative permittivity and the conductivity of the surface, ω the angular frequency and ϵ_0 the permittivity of vacuum. If necessary, these coefficients may be multiplied by a surface roughness attenuation factor [18]. It is also possible to use the coefficient for a slab of finite thickness [19].

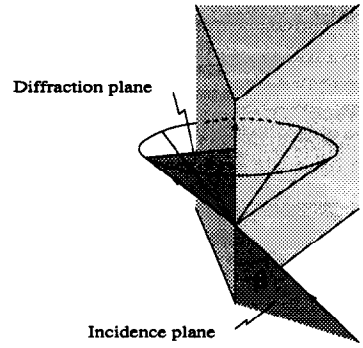

Figure 1. Diffraction by an edge.

For the diffraction case a difficulty arises because of the unavailability of an exact analytical expression for the dyadic coefficient when the conductivities of materials are finite. Two expressions for coefficients including finite-conductivity are the heuristic coefficient [19–21] and the impedance wedge coefficient [22]. The problem with the first one is that it does not provide correct results for certain combinations of incident and diffracted ray orientations, nor does it when incidence is oblique. On the other hand, the impedance wedge coefficient (derived from Maxwell equations) has not been developed yet in a practical form for the case of oblique incidence, and takes about 2.5 times more computation time than the heuristic coefficient. Considering that the errors introduced by the use of the latter are not too consequential since they occur away from optical boundaries (where the diffracted field is less important), it has been chosen for the prediction.

The dyadic heuristic diffraction coefficient can be found in [20] for the case of normal incidence. To deal with the case of oblique incidence (which occurs in the prediction), a $\sin\beta$ factor is heuristically included in the denominator (β being the angle between the edge and the incident ray, as shown on Figure 1). Cross-polarization terms are neglected. These approximations are acceptable provided that β is not too far from ninety degrees.

2.3. Impulse Response and Received Power

Ray techniques allow to express the channel characteristics in terms of ray contributions, which are computed using the dyadic reflection and diffraction coefficients and the antenna patterns (including amplitude and phase). These can be written in a compact form, with the following assumptions:

- a path between the transmitting and receiving antennas may include a finite number of reflections on walls (which are assumed plane and vertical), floor and ceiling (which are assumed plane and horizontal) and diffractions on vertical edges. The angle between the vertical walls may be arbitrary.
- the antennas are located anywhere between the walls, floor and ceiling. Their orientations, patterns and polarization are arbitrary.
- only the first-order diffraction term is considered (not the slope-diffraction term). When there are multiple diffractions in a path, it is assumed that no diffracting edge lies in the transition region of a previous diffraction.

Under the above assumptions, the most general expression for the received power P_R, valid in all cases, is given by:

$$\frac{P_R}{P_T} = \frac{g_R g_T}{4k^2} |\sum_n K_n|^2 \tag{4}$$

$$\tag{5}$$

The equivalent baseband impulse response $h(t)$ is written as:

$$h(t) \sim \sum_n K_n b(t - \tau_n) \tag{6}$$

where P_T is the transmitted power, g_R and g_T are the gains of the receiving and transmitting antennas respectively, k is the wavenumber, and $b(t)$ is a baseband impulse. Equation 6 may be recognized as Turin's formulation [23] for the radio channel. The parameters K_n and τ_n represent the contribution due to the n^{th} path:

$$K_n \equiv \underline{\mathbf{f}}_T(\theta_{Tn}, \phi_{Tn}) \cdot \bar{C}_n \cdot \underline{\mathbf{f}}_R(\theta_{Rn}, \phi_{Rn}) A_n e^{-jkL_n} \tag{7}$$

$$\tau_n \equiv L_n/c \tag{8}$$

In the above equations, c is the velocity of light, $\underline{\mathbf{f}}_T(\theta_{Tn}, \phi_{Tn})$ and $\underline{\mathbf{f}}_R(\theta_{Rn}, \phi_{Rn})$ are the pattern functions for the transmitting and receiving antennas (respectively), evaluated for the appropriate angles. The dyadic parameter $\bar{C}_n$ is a product of reflection and diffraction coefficients. As an example, the writing of the parameter $\bar{C}_n$ for a n^{th} path which consists of three reflections and one diffraction is as such:

$$\bar{C}_n \equiv \bar{R}_n^{(1)} \cdot \bar{R}_n^{(2)} \cdot \bar{D}_n^{(1)} \cdot \bar{R}_n^{(3)} \tag{9}$$

It is understood that the exact order and number of reflections and diffractions depends on the particular path, and each coefficient depends on the rays orientations, the material and the frequency. For the direct path ($n = 0$), $\bar{C}_0$ reduces to unit value. The spatial attenuation factor A_n depends on the total path length L_n and the path lengths $\{r_n^i\}$ between each point of diffraction on the n^{th} path:

$$A_n = \sqrt{\frac{1}{L_n \prod_{i=0}^{N} r_n^i}} \tag{10}$$

3. Ray Tracing Algorithm

3.1. PRINCIPLES

The step of elaborating an efficient method to compute the most significant paths between the transmitter and the receiver is crucial, as this determines for a great part the computation time necessary to get the results. To be efficient, the method should use a maximum of *a priori* information about the structure of the environment. In the present case, this information is contained in the assumption, formulated in the preceding section, that the walls are vertical and that the floor and the ceiling are horizontal. Most indoor environments have this overall regular pattern, except maybe at certain sites like staircases. Alternate method have been proposed for the case of UHF propagation and could possibly deal with more general geometries [11],

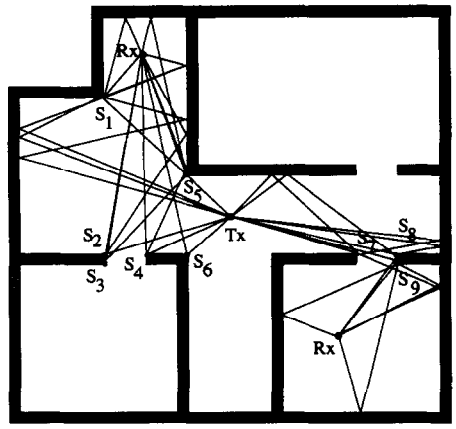

Figure 2. Projected ray paths for a complex site (S_j stand for diffraction sources).

the resultant gain in flexibility being obtained at the price of computer efficiency. The method should depend also on the interaction mechanisms that are taken into account - in this case the reflection and diffraction mechanisms.

The regular structure of the environment allows the separation of the problem of computing the paths in the three-dimensional space in two simpler problems, namely the computation of the projections of the paths in the horizontal plane (a 2D problem), and then on the vertical axis (a 1D problem). In particular, the computation of the diffracted paths is much more simpler in a horizontal cut where the edges reduce to points. This separation is possible because 1) the horizontal components of the paths remain unchanged after a reflection on the floor or the ceiling, 2) the vertical component remains unchanged after a reflection on a vertical wall or a diffraction on a vertical edge, and 3) the walls go from the floor to the ceiling. Properties 1) and 2) are easily shown using reflection and diffraction laws [22]. The approach is therefore to first compute all possible projections of the paths in the horizontal plane, and then to compute the vertical components, taking into account antennas and ceiling heights, the number of reflections on the floor and the ceiling that are considered and the total unfolded path length in the horizontal plane. The three-dimensional path is thus completely determined, and its contribution to the channel characteristic of interest may be computed using equation 7.

Figure 2 shows a horizontal cut of a typical configuration of an indoor environment. The transmitter is located at the center, and two possible receiver positions are shown with some projected paths. The procedure to obtain all possible projected paths (including any number of reflections and diffractions) between the transmitter and a receiver is as follow: all possible sub-paths are computed from the transmitter or a diffracting edge (source) to a receiver or another diffracting edge (destination). These sub-paths, which may include a number of reflections, are then linked to include diffractions on edges.

The sub-paths between a source and a destination (including reflections) could be computed using a classic image method like in [3]. However, a direct application of this method would be inefficient because many images are invisible (since transmission through walls is considered negligible) and would be computed uselessly. The method proposed here is based on the fact that the visibility region of an image, in a two-dimensional space where transmission through segments (walls) can be omitted, is delimited by a polygon. That polygon can be determined from the visibility region (polygon) of an image of lower order, allowing a recursive computation which is explained next.

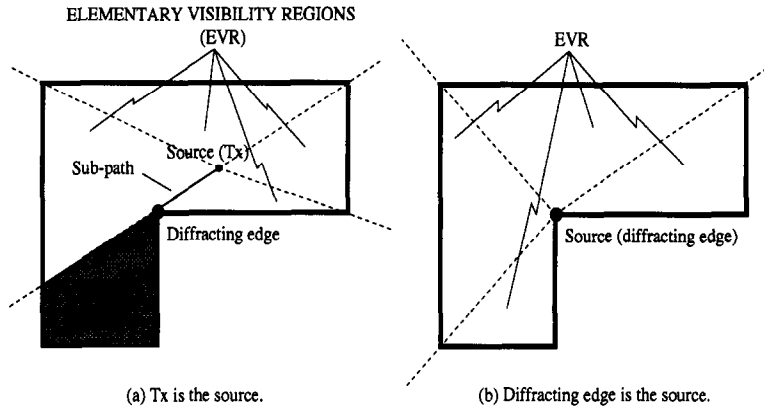

Figure 3. First step of EVR computation process.

The process starts with the source, whose visibility region is determined by splitting the surrounding region by half-lines originating from its position and intersecting the edges visible from it. The sub-paths whose destination is a diffracting edge, (without reflection) are found at the same time. This is illustrated on Figure 3 for a simplified configuration, where the source is either the transmitter or a diffracting edge. After the splitting is completed, each region, called *elementary visibility region* (EVR), is delimited by two half-lines and a wall. These regions correspond to the possible positions for a receiver having a direct sub-path between itself and the source.

The visibility region of a first-order image is then computed from the EVR with the corresponding reflecting wall. The same splitting process is performed, replacing the source by the image and considering this time the region delimited by the reflected half-lines and the reflecting wall. The sub-paths whose destination is diffracting edge and including one reflection onto the wall are also found (Figure 4). The new EVRs (associated with the image) correspond to the possible positions for a receiver having a one-reflection sub-path between itself and the source. The process continues for higher-order images, until some threshold is reached. The exact definition of this threshold may change depending on the implementation. A trivial example would be to stop after a fixed number of reflections (image order). However, it is better to compute a reflection loss estimate for each EVR when the variations in the electrical properties of walls are important in the environment of interest.

The sub-paths whose destination is the receiver are determined by checking which visibility regions include its position. It is thus advantageous to store EVRs in memory when more than one receiver position is considered, as in a path loss mapping computation. The sub-paths whose destination is a diffracting edge are determined during the EVR computation process, using efficiently the *a priori* information that a vertical diffracting edge is always at the boundary between two walls.

3.2. Implementation

Two applications of the above algorithm have been coded in C++. In the first, the path loss mapping (coverage) is generated for a specified position of the transmitting antenna and a specified height of the receiving antenna. For each position P_c of the receiving antenna, a local

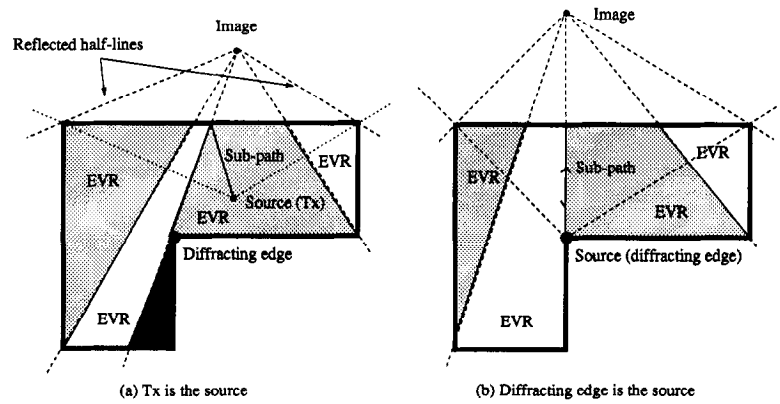

Figure 4. Second step of EVR computation process.

average of the received power $< P_R >$ is computed using the following approximation:

$$\frac{< P_R >}{P_T} \approx \frac{g_R g_T}{4k^2} \sum_n |K_n(P_c)|^2 \tag{11}$$

In the second application, the channel baseband complex impulse response is computed for specified positions of the receiving and transmitting antennas, using equation 6 with a chosen pulse $b(t)$. Both applications take a configuration file as input which contains information about position and electrical properties of walls, floor and ceiling, and the edges on which diffraction is considered. The EVRs associated with each source are first computed along with the sub-paths whose destination is a diffracting edge, as described above. Then a receiver position is specified and the sub-paths whose destination is the receiver are computed from the EVRs. This allows the computation of the three-dimensional paths and their contributions for this particular receiver position. When the receiver position is changed, the sub-paths whose destination is the receiver are computed from the same EVRs, thus avoiding useless recomputations.

4. Results

4.1. Coverage Prediction

As an example of coverage prediction computation, the path loss mapping has been generated for the fictitious complex site of Figure 2 at 37.2 GHz. Site dimensions were selected to be 10 m x 10 m, constitutive parameters were arbitrarily fixed at $\epsilon_r = 3.5$ and $\sigma = 10^{-7}$ S/m, for all walls, floor and ceiling, to obtain a reflection loss of about 10 dB at normal incidence. The transmitter is at center of the site and at a height of 2 m and the receiver is at a height of 1.75 m. Both transmitting and receiving antennas are omnidirectional vertically polarized dipoles with a cosine-shaped field pattern in the vertical plane. Local averages of the received power $< P_R >$ are computed for 2500 locations (for the receiving antenna) on an area of 100 m^2, which means a point for every 20 cm. Figure 5 shows the path loss mapping computed taking into account a maximum of one diffraction on exterior edge by path. The mapping is represented by a pseudocolor plot on part (a) and by a mesh surface on part (b).

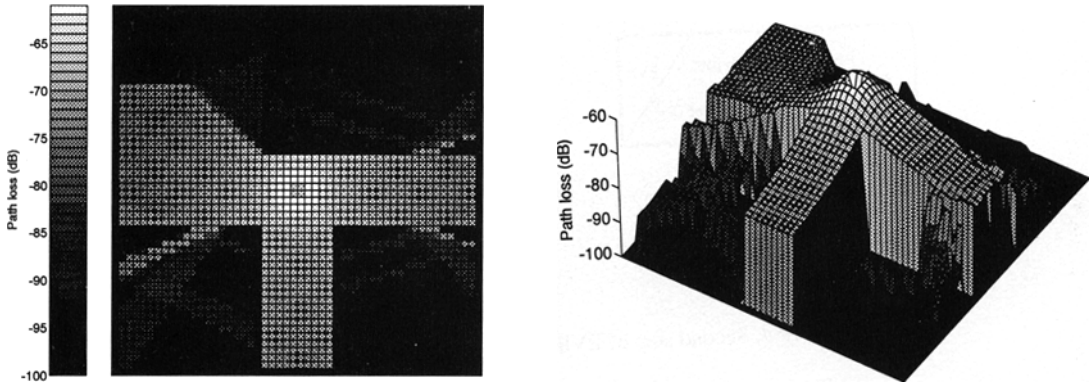

(a) Pseudocolor representation.

(b) Mesh surface representation.

Figure 5. Path loss mapping for the fictitious site of Figure 2.

4.2. WIDEBAND RESULTS

To ascertain the validity of the model, comparisons between predicted and available measured impulse responses have been done for the site illustrated on Figure 6. This site consists in an empty simple parallelepipedic room and a more complex room which contained furniture such as tables and chairs. Only the important structures (Faraday cage, air-conditioner) were included for the prediction. As electrical properties of materials are not easily available at 37.2 GHz, UHF values were used instead as shown on Table 1. The measurement system is shown on Figure 7 and more details are available in [13]. A vertically polarized omnidirectional antenna and a 15 dB gain horn antenna with an approximate 3-dB beamwidth of 24° over the whole waveguide band (26-40 GHz) were used at the receiver and the transmitter respectively. An averaging over many orientations (in the horizontal plane) for the horn antenna was done by fitting a regression curve through the multiple measurement values obtained over many courses for each room to eliminate the effect of directivity, and both antennas were at 1.56 m height. To represent these special conditions in the predictions, it has been decided to consider that both antennas are omnidirectional and to include no reflection on floor or ceiling (because of the horn antenna directivity). The impulse responses are computed using 5 ns-width gaussian pulses, which corresponds to the bandwidth used in the experimentation, and an averaging of 25 responses computed on a small region around each location is done to reduce variations due to fading effects.

Figures 8 and 9 show the predicted and measured power delay profiles for specified locations of the transmitter and the receiver. The experimental profile is time-shifted and power-normalized to fit its first peak with the predicted first peak, since absolute received power and time delay were not measured. The validity of the prediction is thus appreciated by comparing the other peaks and the RMS delay spreads, the latter being shown on Table 2.

As far as the delays are concerned, comparisons between predicted and measured curves show that most predicted and measured paths correspond. The second and third group of paths

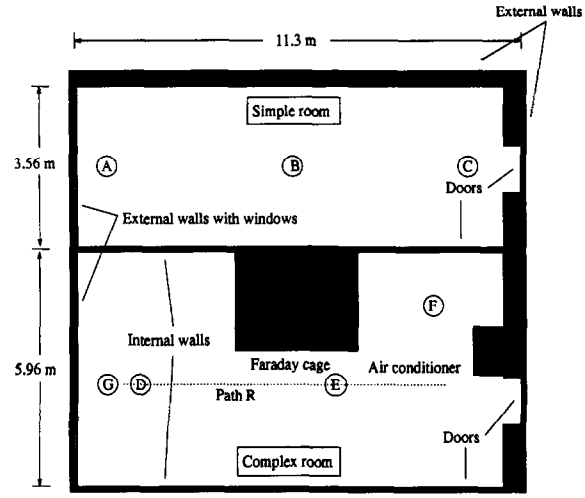

Figure 6. Site for measurements.

Table 1. Electrical properties of specified surfaces used in the prediction.

Surfaces	Rel. permittivity.	Conductivity (S/m)
External Wall	15	10^{-5}
Internal Wall	14	10^{-7}
Faraday Cage	1	10^{7}
Air Conditioner	2	10^{4}
External Wall with Windows	8	10^{2}
Floor (ciment tile)	1	0.005
Ceiling (metallic tile)	2	0.01

are well predicted on figures 8(a) and 8(b). Figure 9(a) also shows good agreement for the path delays. In amplitude, the inaccuracies appears to be more important and may be attributed to the lack of precise information about material properties. Significant discrepancies between

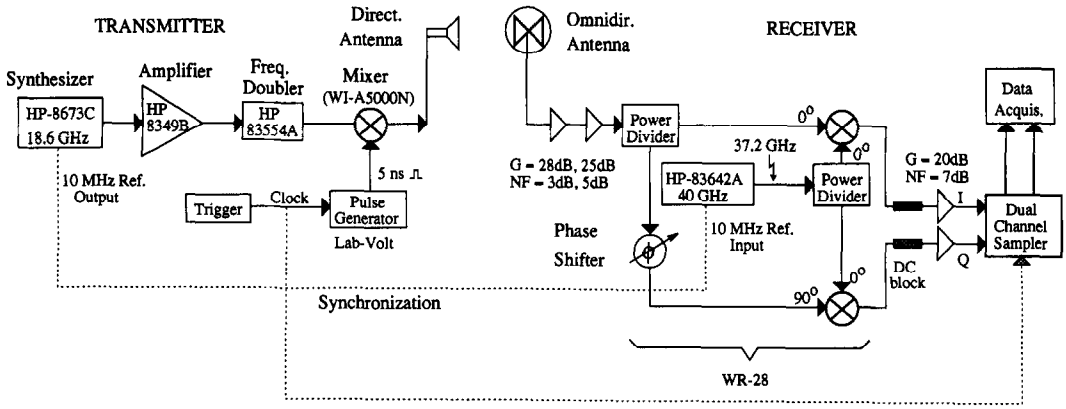

Figure 7. Impulse response measurement system.

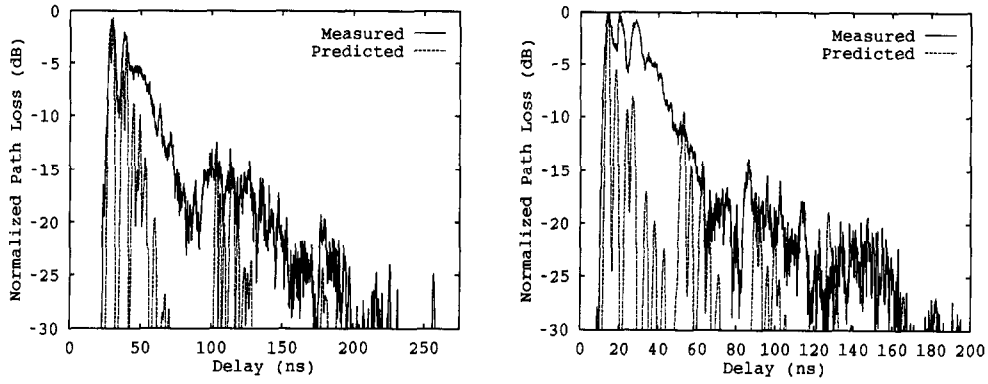

(a) Tx at location A, Rx at location C.

(b) Tx at location B, Rx at location C.

Figure 8. Predicted and measured power delay profiles in the simple room.

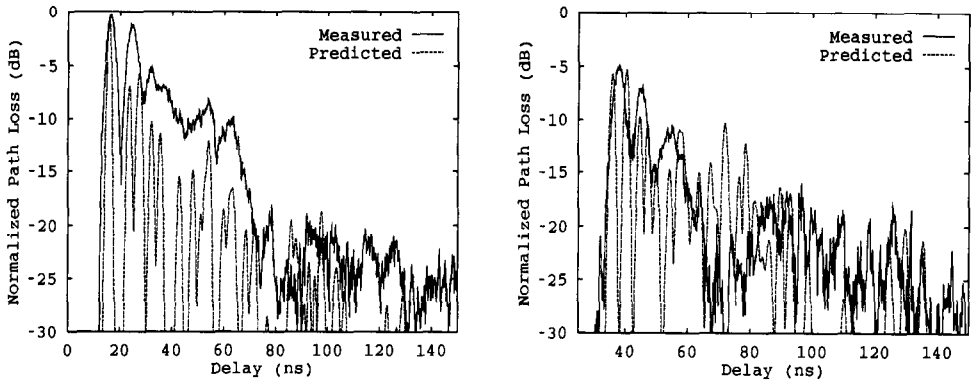

(a) Tx at location D, Rx at location E.

(b) Tx at location D, Rx at location F.

Figure 9. Predicted and measured power delay profiles in the complex room.

prediction and measurements are observed when the receiver lies in the shadow of the Faraday cage, as shown on Figure 9(b). This can be explained least in part by errors consecutive to the averaging over many measured responses. It should be noticed that the shortest path, which is

Table 2. Measured and predicted RMS delay spread for specified Tx and Rx locations.

Tx pos.	Rx pos.	Predicted (ns)	Measured (ns)
A	C	22.0	30.0
B	C	22.5	20.1
D	E	18.8	19.9
D	F	19.8	24.7

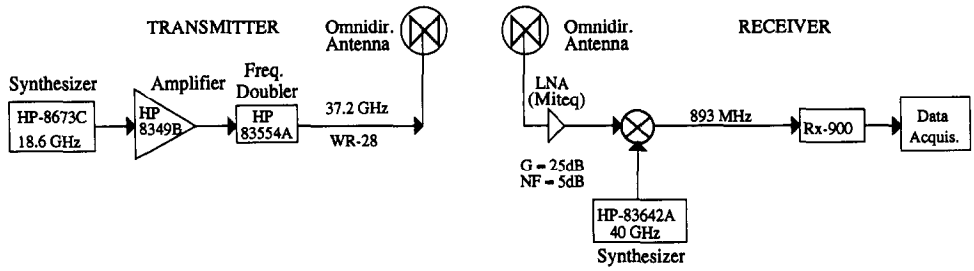

Figure 10. CW measurement system.

a diffracted one, is far from being the strongest. This effect is accentuated by the presence of a metallic structure (Faraday cage) onto which lossless reflections can take place.

4.3. Narrowband Results

Further validation of the model can be done by comparing experimental and predicted results in the narrowband case. CW measurements have been performed using the system [13] shown on Figure 10. Both antennas are vertically polarized, omnidirectional, and at 1.40 m height. A sample was taken at every 0.9 mm. The prediction included a maximum of one reflection on floor or ceiling and the signal level was computed for each 2 cm. For this result, the ray contributions are coherently added (equation 4) to observe small-scale fading, in contrast with coverage prediction computations where the signal power is locally averaged. Figure 11 shows the predicted and measured received signal level for the scenario shown on figure 6 where the transmitter is fixed at location G and the receiver follows the path R. It is observable that the two signals follow the same trend, although they do not agree on small scale fluctuations. This behavior was foreseeable since the predicted and measured samples do not coincide with sufficiently high precision, considering that the wavelength is only 8 mm. In this situation, the distribution functions for the two signals provide a good criterion for comparison. Figure 12 shows the distribution functions for the two signal levels normalized by their respective RMS values. It can be seen that the distributions are in good agreement, especially for high signal levels.

The CPU time required by this technique is strongly dependent on the number of walls, diffracting edges and obviously the results accuracy to reach. For the above result (complex room), which considers 20 walls (including floor and ceiling) and 6 diffracting edges, an average number of about 37000 paths were computed for each mapping point (receiver position), requiring about 137 seconds of CPU on a Personal DECstation 5000/20. However, if the number of computed paths is reduced to 1000, the CPU time does not exceed more than 3.3 seconds for each mapping point resulting in only 1 dB decrease in the prediction accuracy. This is sufficiently small to allow a practical application for this technique in real system engineering. The memory space requirements are only 2.7 Mb for the prediction using 37000 paths.

5. Conclusion

An accurate and efficient prediction tool for the characterization of the indoor wireless mm-wave channel has been described. The model can predict the coverage for a given position of the transmitter and the impulse responses for given positions of the receiving antennas in

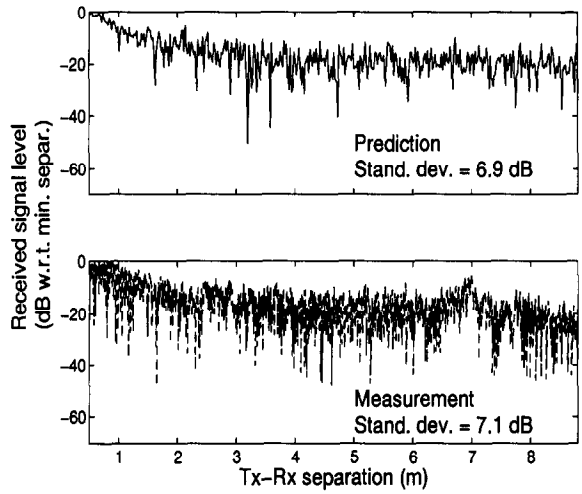

Figure 11. Predicted and measured received signal levels in the complex room.

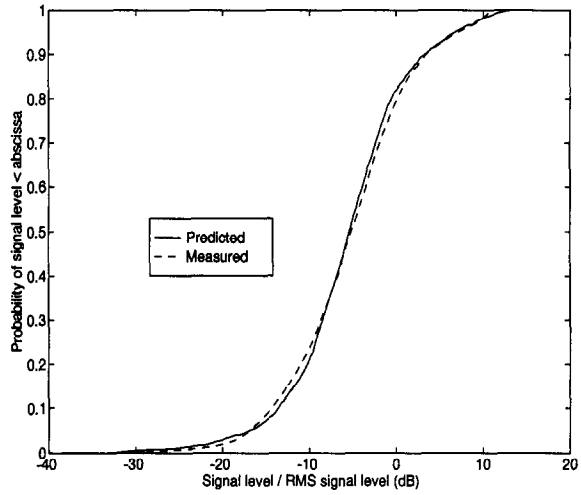

Figure 12. Predicted and measured distribution functions for the received signals.

an user-specified environment. Reflection and diffraction phenomena are taken into account using ray techniques (GO and UTD). An efficient method for the computation of significant paths between the antennas has been elaborated. That 3D ray tracing algorithm uses as much as possible *a priori* information about the structure of the environment. Coverage maps have been generated for a fictitious complex configuration and site by site comparisons between predicted and measured impulse responses have demonstrated the validity of the model despite the lack of information about electrical properties of typical indoor materials at the frequencies of interest. Narrowband results show satisfactory agreement between prediction and measurements.

Acknowledgements

This work has been supported by the Natural Sciences and Engineering Research Council of Canada.

References

1. A. A. M. Saleh and R. A. Valenzuela, "A Statistical Model for Indoor Multipath Propagation," IEEE J. Select. Areas Commun., vol. SAC–5, pp. 128–137, 1987.
2. W. Hocharenko, H. L. Bertoni, J. L. Dailing, J. Qian and H. D. Yee, "Mechanisms Governing UHF Propagation on Single Floors in Modern Office Buildings," IEEE Trans. Veh. Technol., vol. VT–41, pp. 496–504, 1992.
3. J. W. McKown and R. L. Hamilton, "Ray Tracing as a Design Tool for Radio Networks," IEEE Network Magazine, vol. 5, no. 6, pp. 27–30, 1991.
4. T. Holt, K. Pahlavan and J. F. Lee, "A Graphical Indoor Radio Channel Simulator Using 2D Ray Tracing," in Proc. 3rd International Symposium on Personal, Indoor and Mobile Radio Communications, Boston, Mass., pp. 13.2.1–13.2.6, 1992.
5. R. A. Valenzuela, "A Ray Tracing Approach to Predicting Indoor Wireless Transmission," in Proc. 43rd IEEE Vehicular Technology Conference, Secaucus, N.J., pp. 214–217, 1993.
6. G. Yang, S. Li, J.-F. Lee and K. Pahlavan, "Computer Simulation of Indoor Radio Propagation," in Proc. 4th International Symposium on Personal, Indoor and Mobile Radio Communications, Yokohama, Japan, pp. A1.3.1-A1.3.5, 1993.
7. M. Kimpe, V. Bohossian and H. Leib, "Ray Tracing for Indoor Radio Channel Estimation," in Proc. 2nd International Conference on Universal Personal Communications, Ottawa, Canada, pp. 64–68, 1993.
8. D.I. Laurenson, S. McLaughlin and A. U. H. Sheikh, "The Application of Ray Tracing and the Geometrical Theory of Diffraction to Indoor Channel Modelling," in Proc. IEEE Globecom'93, Houston, Texas, pp. 1242–1246, 1993.
9. G. Yang, K. Pahlavan, and J. F. Lee, "A 3D Propagation Model with Polarization Characteristics in Indoor Radio Channels," in Proc. IEEE Globecom'93, Houston, Texas, pp. 1252–1256, 1993.
10. C. M. Peter Ho and Theodore S. Rappaport, "Wireless Channel Prediction in a Modern Office Building Using an Image-Based Ray Tracing Method," in Proc. IEEE Globecom'93, Houston, Texas, pp. 1247–1251, 1993.
11. S. Y. Seidel and T. S. Rappaport, "Site-Specific Propagation Prediction for Wireless In-Building Personal Communication System Design," IEEE Trans. Veh. Technol., vol. VT–43, pp. 879–891, 1994.
12. M. C. Lawton and J. P. McGeehan, "The Application of a Deterministic Ray Launching Algorithm for the Prediction of Radio Channel Characteristics in Small-Cell Environments," IEEE Trans. Veh. Technol., vol. VT–43, pp. 955–969, 1994.
13. L. Talbi and G. Y. Delisle, "Wideband Propagation Measurements and Modeling at Millimeter Wave Frequencies," in Proc. IEEE Globecom'94, San Fransisco, Cal., pp. 47–51, 1994.
14. P. F. M. Smulders and A. G. Wagemans, "A Statistical Model for the Mm-wave Indoor Radio Channel," in Proc. 3rd International Symposium on Personal, Indoor and Mobile Radio Communications, Boston, Mass., pp. 10.1.1–10.1.4, 1992.
15. P. F. M. Smulders, "Geometrical Optics Model for Millimetre-Wave Indoor Radio Propagation," Electronics Letters, vol. 29 no. 13, pp. 1174–1176, jun. 1993.
16. P. F. M. Smulders, "Influence of Antenna Radiation Pattern on Mm-wave Indoor Radio Channels," in Proc. 2nd International Conference on Universal Personal Communications, Ottawa, Canada, pp. 631–635, 1993.
17. C. A. Balanis, Advanced Engineering Electromagnetics, Wiley: New York, 1989.
18. R. J. Luebbers, "A Heuristic UTD Slope Diffraction Coefficient for Rough Lossy Wedges," IEEE Trans. Ant. Propagat., vol. 37, no. 2, pp. 206–211, 1989.
19. W. D. Burnside and K. W. Burgener, "High Frequency Scattering by a Thin Lossless Dielectric Slab," IEEE Trans. Ant. Propagat., vol. 31, no. 1, pp. 104–110, 1983.
20. R. J. Luebbers, "Finite Conductivity Uniform GTD Versus Knife Edge Diffraction in Prediction of Propagation Path Loss," IEEE Trans. Ant. Propagat., vol. 32, no. 1, 1984.
21. R. J. Luebbers, "Propagation Prediction for Hilly Terrain Using GTD Wedge Diffraction," IEEE Trans. Ant. Propagat., vol. 32, no. 9, 1984.
22. G. L. James, Geometrical Theory of Diffraction for Electromagnetic Waves, third edition revised, Peregrinus: London, 1986.
23. G. L. Turin, F. D. Clapp, T. L. Johnston, S. B. Fine, and D. Lavry, "A Statistical Model for Urban Multipath Propagation," IEEE Trans. Veh. Technol., vol. VT–21, pp. 1–9, 1972.

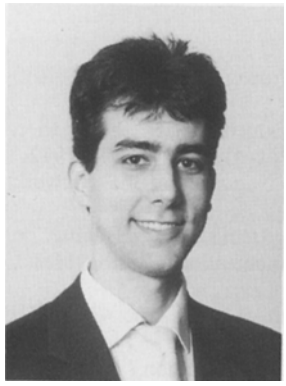

Paul Marinier was born in Montreal, Quebec, Canada, in 1971. He received the B.Sc. degree in physics from University of Sherbrooke, Quebec, Canada in 1992. After graduation he joined the personal communications systems group at INRS-Telecommunications, Verdun, Quebec, Canada, from which he obtained the M.Sc. degree in telecommunications in 1994. He is currently pursuing a Ph.D. degree at this same institution. He holds a Natural Sciences and Engineering Research Council of Canada (NSERC) postgraduate fellowship. His technical interests are in radiowave propagation and indoor wireless systems.

Gilles Y. Delisle (S'63–M'73–SM'86) has been a Professor of Electrical Engineering at Laval University, Quebec, Canada, since 1973, where he was head of the department from 1977 to 1983. Since June 1992, he is also Director of INRS-Telecommunications, a research institute which is a part of University du Québec. He is involved in research work in radar cross-section measurements and analytical predictions, mobile radio-channel propagation modeling, personal communications, and industrial realization of telecommunications equipment.

Dr. Delisle is a senior member of the Order of Engineers of the Province of Quebec, a member of the board of Examiners of this Society, Canadian President of URSI, ACFAS and a Fellow of the Engineering Institute of Canada. His work in technology transfer has been recognized by a Canada Award of Excellence in 1986. He has been a consultant in many countries and in 1986, he was awarded the J. Armand Bombardier prize of ACFAS (Association Canadienne Française pour l'Avancement des Sciences) for outstanding technical innovation.

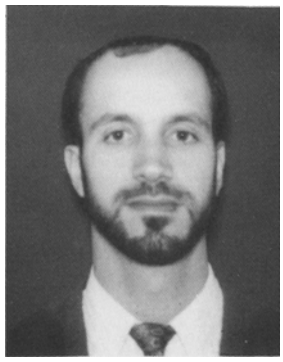

Larbi Talbi was born in Bejaia, Algeria in July 1962. He received is engineer diploma from the Institut National d'Enseignement Supérieur d'Electronique de SETIF, Algeria in 1986. In 1987, he joined the electrical engineering deparment of Laval University where he successively got his Master degree in 1989 and his Ph.D. diploma in 1994. He completed a Post-Doctoral at INRS-Télécommunications in October 1995 and he is member of the teaching staff at the College of Technology, Riyadh in Saudi Arabia. His research interests are in numerical methods, radar cross-sections and RF channel characterization and measurements.